

Kondo cooling in quantum impurity systems

Xiangzhong Zeng,¹ Lyuzhou Ye,¹ Long Cao,¹ Rui-Xue Xu,¹ Xiao Zheng,^{1,*} and Massimiliano Di Ventra^{2,†}

¹*Department of Chemical Physics, University of Science and Technology of China, Hefei, Anhui 230026, China*

²*Department of Physics, University of California, San Diego, La Jolla, California 92093, USA*

(Dated: Submitted on March 15, 2022)

The Peltier effect is the reverse phenomenon of the Seebeck effect, and has been observed experimentally in nanoscale junctions. However, despite its promising applications in local cooling of nanoelectronic devices, the role of strong electron correlations on such a phenomenon is still unclear. Here, by analyzing the thermoelectric properties of quantum impurity systems out of equilibrium, we unveil the essential role of electron-electron interactions and quantum resonant states in Peltier cooling, leading to the prediction of the *Kondo cooling* phenomenon. The existence of such Kondo cooling is validated by a reverse heat current and a lowered local temperature in a model junction. The discovery of this unconventional Peltier cooling offers a new approach toward nano-refrigeration, and highlights the unique role of strong electron correlations in nonequilibrium quantum systems.

Introduction.— The Peltier effect is a fundamental thermoelectric phenomenon. It means that when an electric current is passed through a junction connecting two conductors (A and B), heat will be transferred from A to B, which may lead to cooling in A. Peltier refrigerators [1, 2] have been designed and applied to cool various types of electronic devices [3–8]. This is very appealing for practical purposes, because otherwise the local heat generation and accumulation will likely deteriorate the performances of, or cause damages to the electronic devices.

In the past decade, Peltier cooling in nanoscopic systems has attracted enormous theoretical [9–18] and experimental [19–28] efforts. Thanks to the impressive advances in the synthesis, fabrication and manipulation of nano-sized materials, Peltier cooling has been realized in molecular junctions [19–21, 27, 28], organic thermoelectric flakes [22, 26], and ferromagnetic/ferrimagnetic metal films [23–25]. For instance, Cui *et al.* have directly observed the Peltier cooling in gold junctions with conjugated molecules, and also revealed the relationship between cooling and electron transport characteristics [21].

Despite the remarkable progress, the strength of cooling in nanojunctions has not met the needs of practical applications. For instance, the measured cooling power in Ref. [21] is lower than 1 nanowatt, thus leaving plenty of room for improvement. Theoretically, the Peltier effect in nanojunctions has been explored within the Landauer theory of quantum transport [11, 21, 29–41]. However, the cause of the limited cooling magnitude is largely unclear. Moreover, although the influence of electron-electron interactions and the presence of quantum resonant states on local heating of nanojunctions was widely studied [10, 42–44], how these features affect the Peltier cooling has remained a topic barely touched upon.

To shed light on the above effects, and to provide new clues to enhancing Peltier cooling, in this Letter we investigate the thermoelectric response of prototypical quantum impurity systems to applied voltages by means of theoretical analysis and numerical simulations. Particularly, to accentuate the possible role of quantum reso-

nance and electron correlations, we shall focus on systems which explicitly involve electron-electron interactions, while the influence of phonons is omitted. We then predict an unconventional Peltier effect, we call *Kondo cooling*, which is the direct result of electron correlations. This phenomenon can be readily verified experimentally and offers a new path toward nano-refrigeration.

Peltier cooling with Kondo resonant states.— Let us first provide a simple analytical picture of the Kondo cooling phenomenon. Without loss of generality, the nanojunctions are represented by a number of localized impurities embedded between two leads. We first clarify that the electronic Peltier cooling cannot exist in a single-impurity junction. This is because when an electron is driven by a bias to traverse the junction, it gains energy from the work done by the electric field. Such excess energy must dissipate into the surrounding (leads) in the form of heat to conserve energy and thus sustain the stationary state of the junction. Consequently, a single impurity in the junction has no choice but to behave as a hot spot to release the heat. In contrast, if there is more than one impurity in the junction, it is possible to have one impurity cooled down by the Peltier effect, at the expense of heating up the other impurity. For the sake of discussion, we then consider a junction consisting of two impurities connected serially to two metallic leads; see Fig. 1.

By driving a steady electric current I through the junction, the heat current produced by the Peltier effect is $J^P = (\Pi - \Pi_{\text{lead}})I \approx \Pi I$ [20], where Π and Π_{lead} are the Peltier coefficients of the two-impurity complex and the leads, respectively, and usually $|\Pi_{\text{lead}}| \ll |\Pi|$ [7]. Meanwhile, the impurities are also subject to Joule heating with the power $J^J = IV$, which is caused by electron scattering within the impurities or at the impurity-lead interfaces. Thus, in the context of Fig. 1, the net heat currents flowing into the two leads are

$$J_L = J_L^J - J^P \quad \text{and} \quad J_R = J_R^J + J^P, \quad (1)$$

where $J_L^J = I(\bar{\mu}^* - \mu_L)/e$ and $J_R^J = I(\mu_R - \bar{\mu}^*)/e$ are

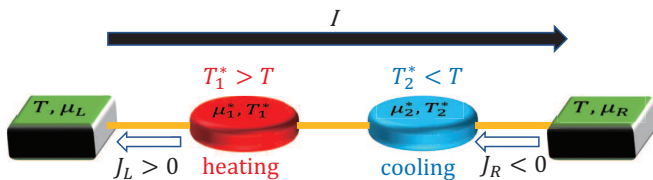


FIG. 1. Schematic illustration of a nanojunction consisting of two localized impurities of identical energetic structure, which are serially connected to two leads (L and R) at a same background temperature T . With a voltage V applied across the junction, the difference in electrochemical potential of the two leads ($\mu_R - \mu_L = eV$) induces an electric current I flowing through the junction. Because of the Peltier effect, impurity-2 has a lower local temperature than the leads ($T_2^* < T$), whereas impurity-1 is heated up ($T_1^* > T$). This corresponds to a net heat flow from impurity-1 to lead- L ($J_L > 0$) and from lead- R to impurity-2 ($J_R < 0$), respectively.

the Joule heat dissipated into the L and R leads, respectively, with $\bar{\mu}^* = (\mu_1^* + \mu_2^*)/2$, and μ_1^* and μ_2^* being the local electrochemical potentials of the impurities 1 and 2. As depicted in Fig. 1, the cooling of impurity-2 is indicated by a local temperature [48, 49], T_2^* , lower than the background temperature T , of the leads ($T_2^* < T$), as well as a reverse heat current flowing from lead- R to impurity-2, i.e.,

$$J_R = I(V/2 + TS) < 0. \quad (2)$$

Here, the voltage drop is assumed to be antisymmetric across the junction, and we have used the second Thomson relation $\Pi = TS$ [3, 4, 6], with S being the thermopower (or Seebeck coefficient) [45–47] of the two-impurity complex [50, 51]. Clearly, a large negative S is an essential prerequisite for the cooling of impurity-2.

The zero-bias thermopower can be expressed by the following Landauer-like formula [52, 53] (consider the wide-band limit for the leads and set $e = \hbar = k_B = 1$)

$$S = -\frac{1}{T} \frac{\int d\omega (\omega - \mu) f'_\beta(\omega) A(\omega)}{\int d\omega f'_\beta(\omega) A(\omega)}. \quad (3)$$

Here, $A(\omega)$ is the normalized spectral density of the impurities, $f_\beta(\omega)$ is the Fermi function, and $f'_\beta(\omega) \equiv \frac{\partial f_\beta(\omega)}{\partial \omega}$ defines a thermal activation window, which is centered at the equilibrium chemical potential μ and the width is determined solely by T [53]. The value of S under a zero or low bias is thus dictated by the lineshape of $A(\omega)$ within such a thermal energy window.

In general, a quantum resonant state is manifested by a single spectral peak in $A(\omega)$. From Eq. (3), it is clear that a sharp resonance peak located within the left (right) half of the thermal activation window will contribute a significant positive (negative) value to S . Besides, resonant states also provide ballistic channels for the electron transport, leading to an increased I . Therefore, quantum

resonant states located slightly off the lead chemical potential tend to boost a reverse heat current, and hence will greatly enhance the Peltier cooling.

Among the various types of quantum resonant states, those arising due to strong electron correlations are particularly intriguing, since a low background temperature is typically required to suppress the thermal fluctuations which impair the electron correlations. Therefore, by exploiting the concomitant effect of Peltier cooling and strong electron correlations, it is possible to create a local spot that is cooler than the already cool surrounding.

As is well known, the screening of a localized spin moment by the conduction electrons in a metallic lead gives rise to spin-Kondo (S-Kondo) states [54–60] at the impurity-lead interface. Their characteristic spectral feature is a sharp resonance peak centered at μ . Because of the symmetric lineshape of the spectral peak, while S-Kondo states enhance the junction conductance [61], they have little influence on the thermopower S [53].

On the other hand, if the electrons are subject to a strong inter-impurity repulsion, the *orbital* moment of the two-impurity complex will behave like a pseudospin, and its interaction with the leads will result in the formation of *orbital-Kondo* (O-Kondo) states [62–68]. The O-Kondo spectral signature is a pair of satellite peaks located on either side of μ (see also below). Based on Eq. (3), the value of S can then be significantly varied by adjusting the relative heights of these two satellite peaks, which can be realized by tuning the energetic structures of the impurities [53].

The above analysis predicts unambiguously that further cooling of an already cool impurity can be realized by invoking O-Kondo states in the junction. In the following, we shall validate such a prediction by performing accurate numerical simulations on a prototypical quantum impurity model.

Model and Methodology.– The total Hamiltonian of the junction assumes the form of an Anderson impurity model (AIM) [69], $\hat{H} = \hat{H}_{\text{imp}} + \hat{H}_{\text{lead}} + \hat{H}_{\text{int}}$. Specifically, the two impurities are described by $\hat{H}_{\text{imp}} = \sum_{\nu=1,2} (\epsilon_\nu \hat{n}_\nu + U \hat{n}_{\nu\uparrow} \hat{n}_{\nu\downarrow}) + U_{12} \hat{n}_1 \hat{n}_2 + [t (\hat{a}_{1\uparrow}^\dagger \hat{a}_{2\uparrow} + \hat{a}_{1\downarrow}^\dagger \hat{a}_{2\downarrow}) + \text{H.c.}]$, where $\hat{n}_\nu = \sum_s \hat{n}_{\nu s} = \sum_s \hat{a}_{\nu s}^\dagger \hat{a}_{\nu s}$, with $\hat{a}_{\nu s}^\dagger$ ($\hat{a}_{\nu s}$) creating (annihilating) a spin- s electron on impurity- ν ; U and U_{12} are the intra- and inter-impurity electron-electron interaction energies, respectively; and t is the hopping integral between the two impurities. $\hat{H}_{\text{lead}} = \sum_{\alpha ks} \epsilon_{\alpha k} \hat{d}_{\alpha ks}^\dagger \hat{d}_{\alpha ks}$ represents the metallic leads, with $\hat{d}_{\alpha ks}^\dagger$ ($\hat{d}_{\alpha ks}$) being the creation (annihilation) operator for orbital- k of lead- α ($\alpha = L, R$); and $\hat{H}_{\text{int}} = \sum_{\alpha ks\nu} t_{\alpha k\nu} \hat{a}_{\nu s}^\dagger \hat{d}_{\alpha ks} + \text{H.c.}$ describes the electron transfer couplings between the impurities and the leads, with $t_{\alpha k\nu}$ being the coupling strengths.

The thermoelectric properties of the junction are determined by a hierarchical equations of motion (HEOM) method [70–76], which has been widely adopted to inves-

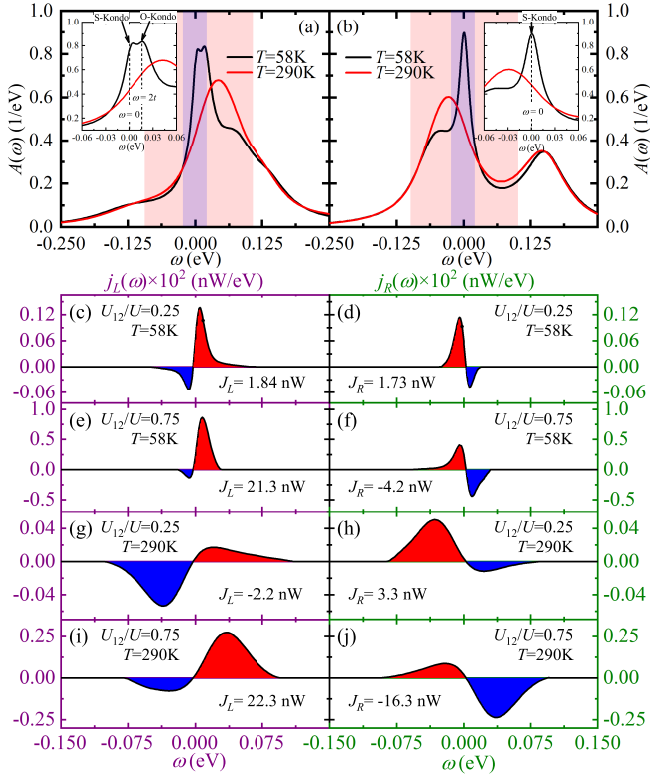


FIG. 2. Normalized spectral function $A(\omega)$ of the two impurities with (a) $U_{12}/U = 0.75$ and (b) 0.25 under zero bias and different background temperatures. The areas shaded in purple and pink mark the thermal activation windows under $T = 58$ K and 290 K, respectively. The insets magnify the S-Kondo and O-Kondo resonance peaks around $\mu = 0$. Panels (c)-(j) depict the heat current spectra $j_\alpha(\omega)$ under an anti-symmetric bias $\mu_R = -\mu_L = V/2 = 0.0025$ eV. The energetic parameters of the AIM are (in units of eV): $U = -2\epsilon_0 = 0.2$, $t = 0.0075$, $\Gamma_{L1} = \Gamma_{R2} = 0.02$, $\Gamma_{L2} = \Gamma_{R1} = 0$, and $W = 1.25$.

tigate strongly correlated quantum impurity systems out of equilibrium [73, 77–80]. In the framework of HEOM, the influence of the metallic leads are fully captured by hybridization functions which assume a Lorentzian form of $\Delta_{\alpha\nu}(\omega) \equiv \pi \sum_k |t_{\alpha k\nu}|^2 \delta(\omega - \epsilon_{\alpha k}) = \frac{\Gamma_{\alpha\nu} W^2}{(\omega - \mu_\alpha)^2 + W^2}$, with $\Gamma_{\alpha\nu}$ being the hybridization strength and W the band width of the leads. The results of HEOM are numerically exact provided that they fully converge with respect to the truncation of the hierarchy [81].

The realization of local cooling at impurity- ν is characterized by two criteria: (i) a reverse (negative) heat current flowing into impurity- ν from lead- α , $J_\alpha < 0$, whose magnitude represents the power of Peltier cooling; and (ii) a lower local temperature T_ν^* than the background temperature, as represented by a negative ratio $\gamma_\nu \equiv (T_\nu^* - T)/T < 0$. For the former, the energy spectrum of heat current $j_\alpha(\omega)$ is calculated via the Landauer formula [32, 49] and $J_\alpha = \int j_\alpha(\omega) d\omega$. For the latter, T_ν^* is determined by an operational protocol based on a min-

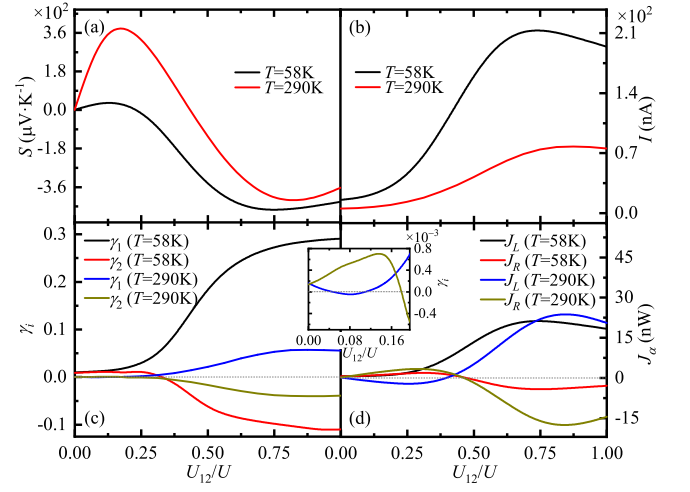


FIG. 3. Evolution of thermoelectric and transport properties with respect to the variation in U_{12}/U : (a) thermopower S , (b) electric current I , (c) local temperature fluctuation γ_ν , and (d) heat currents J_α . Both cryogenic and room temperatures ($T = 58$ K and 290 K) are explored. The inset magnifies the evolution of γ_ν in the small U_{12} region. The energetic parameters of the AIM are the same as those adopted for Fig. 2.

imal perturbation condition (MPC) [44, 48, 49, 82, 83], and the values agree closely to those given by other definitions [84–87] in the low bias region (see also Supplementary Material).

Numerical demonstration of Kondo cooling.— Figure 2(a) depicts the spectral features of Kondo resonant states in the presence of a strong inter-impurity interaction ($U_{12}/U = 0.75$). Under a cryogenic temperature of $T = 58$ K, an S-Kondo peak shows up at $\omega = \mu \equiv 0$. Meanwhile, an O-Kondo peak emerges at $\omega = 2t$, whereas its opposite counterpart at $\omega = -2t$ is invisible. Based on Eqs. (2) and (3), the asymmetric lineshape of $A(\omega)$ around μ will give rise to a large negative S , and hence a reverse heat current from lead- R to impurity-2, i.e., $J_R < 0$. It is thus predicted that impurity-2 is cooled down below the low background T . In contrast, with a much weaker inter-impurity interaction ($U_{12}/U = 0.25$), the O-Kondo signature vanishes almost completely; see Fig. 2(b). The resulting symmetric spectral function around μ will lead to a rather small thermopower S . Consequently, the Peltier cooling is overwhelmed by Joule heating at the both impurities, i.e., $J_L > 0$ and $J_R > 0$.

At room temperature ($T = 290$ K), the Kondo states are completely destroyed. The thermopower S is instead dominated by the non-Kondo resonant state whose spectral signature is a resonance peak located at $\omega \approx \epsilon_0 + U_{12}$. Since the peak center shifts from negative to positive energy as U_{12} strengthens, S will vary from a positive maximum to a negative maximum, leading to the alteration of local cooling site from impurity-1 (negative J_L)

to impurity-2 (negative J_R).

The above prediction on the values of S and the signs of J_α is validated by the calculated nonequilibrium transport properties. Figure 2(c)-(j) display $j_\alpha(\omega)$ under an antisymmetric bias. Under $T = 58$ K, $j_\alpha(\omega)$ distribute tightly around zero energy, where Kondo resonant states contribute predominantly to the electron and heat transport. Particularly, in the case of a strong U_{12} , negative $j_R(\omega)$ is promoted in the energy range spanned by the O-Kondo spectral peak; see Fig. 2(f). In contrast, under $T = 290$ K, $j_\alpha(\omega)$ distributes over a broader energy range, with large negative values emerging at around $\omega \approx \epsilon_0 + U_{12}$.

Figure 3 gives an overview of how the Peltier cooling is enabled by varying U_{12} . Under a cryogenic temperature, a strengthened U_{12} leads to an enhanced O-Kondo resonance, which in turn elevates the thermopower and conductance of the junction. The resultant Kondo cooling of impurity-2 is confirmed by the fact that both the two criteria, $\gamma_2 < 0$ and $J_R < 0$, are met with a sufficiently large U_{12} ; see Fig. 3(c) and (d). Since the MPC-based protocol for the determination of T_2^* does not require any information on heat currents, γ_2 and J_R are calculated independently. It is thus remarkable that the variation of γ_2 with respect to U_{12} exhibits a very similar trend to that of J_R , albeit with a slightly different turning point from heating to cooling.

Local cooling also happens when the Kondo states are all quenched at room temperature. Figure 3(c) and (d) reveal the same trend with impurity-1 subject to marginal cooling with a weak U_{12} , while the cooling site shifts to impurity-2 with a sufficiently strong U_{12} . This verifies the above prediction on the alternation of the local cooling site.

Unlike Kondo resonant states whose energies are intrinsically pinned to the leads' chemical potential, the positions of non-Kondo resonance peaks depend sensitively on the molecular orbital energies of the embedded impurities. Therefore, to have prominent non-Kondo cooling in practical applications, it is essential to shift the resonance energies, such as the energy of the highest occupied molecular orbital (HOMO) or lowest unoccupied molecular orbital (LUMO) of a molecular device, into the thermal activation window. In contrast, the key to realizing conspicuous Kondo cooling is to produce strong O-Kondo resonant states which distribute asymmetrically with respect to the leads' chemical potential.

To explore the full range of external conditions under which the Peltier cooling occurs, we plot in Fig. 4 the heat currents scaled by the thermal energy, J_α/T , as a function of T and V . Clearly, the cooling regions (shaded in blue) exhibit distinct patterns in the cases of weak and strong U_{12} . In the former case, local cooling takes effect at impurity-1 (corresponding to a positive S) within a rather narrow range of T and V ; see Fig. 4(b). There, the cooling arises entirely from non-Kondo resonance. The

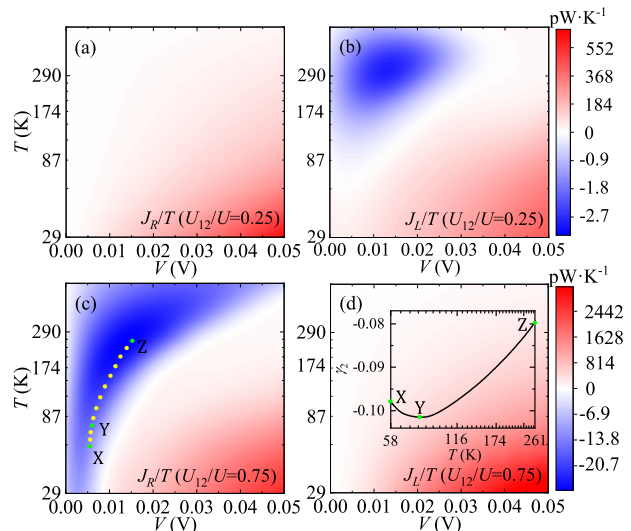


FIG. 4. (a) J_R/T and (b) J_L/T as a function of T and V with $U_{12}/U = 0.25$; and (c) J_R/T and (d) J_L/T as a function of T and V with $U_{12}/U = 0.75$. The voltage is applied antisymmetrically across the junction, i.e., $\mu_R = -\mu_L = V/2$. Blue (red) denotes a negative (positive) heat current flowing out of (into) lead- α , indicating local cooling (heating) of the coupled impurity. The inset of (d) depicts the variation of γ_2 along a path marked in (c) which connects the Kondo and non-Kondo cooling regions. The energetic parameters of the AIM are same as those adopted for Fig. 2.

absence of Kondo cooling under a low T is due to the inactive O-Kondo effect. In contrast, with a strong U_{12} , local cooling exists at impurity-2 within a wide range of T and V ; see Fig. 4(c). Nevertheless, Kondo cooling comes into play only in the lower-left corner (low T and low V), since either the intensified thermal fluctuations or the increased mismatch between μ_L and μ_R will quench the Kondo states [33, 88–91].

The crossover from Kondo cooling to non-Kondo cooling is indicated by a path marked in Fig. 4(c) (the dotted line), along which the variation of γ_2 is depicted in the inset of Fig. 4(d). It is remarkable that the Kondo resonance actually gives rise to an even greater relative drop of local temperature than the non-Kondo resonance. Figure 4 thus highlights the important role of O-Kondo resonant states, as they are uniquely efficacious in further cooling of an already cool spot to produce an appreciable cooling power.

Concluding remarks.— In summary, we have predicted an unconventional Peltier cooling phenomenon, *Kondo cooling*, in quantum impurity systems. It arises due to the crucial roles of electron-electron interactions and quantum resonances. We have validated such a prediction numerically on a model junction. The existence of such prominent Kondo cooling is clearly indicated by the reverse heat current and a lowered local temperature, which originate from the *orbital-Kondo* resonant states

distributed unevenly around the chemical potential. This unconventional Kondo cooling phenomenon offers both a new route toward nano-refrigeration and further reveals the importance of strong electron correlations in nonequilibrium quantum systems.

R.X. and X.Z. acknowledge the support from the National Natural Science Foundation of China (Grant Nos. 21973086 and 21633006), the Ministry of Education of China (111 Project Grant No. B18051), and the Fundamental Research Funds for the Central Universities (Grant No. WK2060000018). The computational resources are provided by the Supercomputing Center of University of Science and Technology of China.

* xz58@ustc.edu.cn

† diventra@physics.ucsd.edu

- [1] F. Giazotto, T. T. Heikkilä, A. Luukanen, A. M. Savin, and J. P. Pekola, *Rev. Mod. Phys.* **78**, 217 (2006).
- [2] J. T. Muhonen, M. Meschke, and J. P. Pekola, *Rep. Progr. Phys.* **75**, 046501 (2012).
- [3] D. M. Rowe and C. M. Bhandari, *Modern Thermoelectrics*, Holt Reinhart and Winston, London, 1983.
- [4] G. S. Nolas, J. Sharp, and J. Goldsmid, *Thermoelectrics: Basic Principles and New Materials Developments*, Springer, Berlin, 2001.
- [5] P. E. Phelan, V. A. Chiriach, and T.-Y. T. Lee, *IEEE Trans. Compon. Packag. Technol.* **25**, 356 (2002).
- [6] D. M. Rowe, *Thermoelectrics Handbook: Macro to Nano*, CRC Press, Boca Raton, 2006.
- [7] F. L. Bakker, A. Slachter, J.-P. Adam, and B. J. van Wees, *Phys. Rev. Lett.* **105**, 136601 (2010).
- [8] J. Flipse, F. L. Bakker, A. Slachter, F. K. Dejene, and B. J. van Wees, *Nat. Nanotechnol.* **7**, 166 (2012).
- [9] R. D'Agosta, N. Sai, and M. Di Ventra, *Nano Lett.* **6**, 2935 (2006).
- [10] Z. Huang, F. Chen, R. D'Agosta, P. A. Bennett, M. Di Ventra, and N. Tao, *Nat. Nanotechnol.* **2**, 698 (2007).
- [11] M. Galperin, K. Saito, A. V. Balatsky, and A. Nitzan, *Phys. Rev. B* **80**, 115427 (2009).
- [12] Y.-S. Liu, B. C. Hsu, and Y.-C. Chen, *J. Phys. Chem. C* **115**, 6111 (2011).
- [13] Y. Dubi and M. Di Ventra, *Rev. Mod. Phys.* **83**, 131 (2011).
- [14] C. M. Finch, V. M. García-Suárez, and C. J. Lambert, *Phys. Rev. B* **79**, 033405 (2009).
- [15] J. P. Bergfield, M. A. Solis, and C. A. Stafford, *ACS Nano* **4**, 5314 (2010).
- [16] O. Karlström, H. Linke, G. Karlström, and A. Wacker, *Phys. Rev. B* **84**, 113415 (2011).
- [17] P. Santhanam and S. Fan, *Phys. Rev. B* **93**, 161410(R) (2016).
- [18] A. Saffarzadeh, F. Demir, and G. Kirzenow, *Phys. Rev. B* **98**, 115436 (2018).
- [19] K. L. Grosse, M.-H. Bae, F. Lian, E. Pop, and W. P. King, *Nat. Nanotechnol.* **6**, 287 (2011).
- [20] I. J. Vera-Marun, J. J. van den Berg, F. K. Dejene, and B. J. van Wees, *Nat. Commun.* **7**, 1 (2016).
- [21] L. Cui, R. Miao, K. Wang, D. Thompson, L. A. Zotti, J. C. Cuevas, E. Meyhofer, and P. Reddy, *Nat. Nanotechnol.* **13**, 122 (2018).
- [22] W. Jin, L. Liu, T. Yang, H. Shen, J. Zhu, W. Xu, S. Li, Q. Li, L. Chi, C.-a. Di, and D. Zhu, *Nat. Commun.* **9**, 3586 (2018).
- [23] K.-i. Uchida, S. Daimon, R. Iguchi, and E. Saitoh, *Nature* **558**, 95 (2018).
- [24] R. Das, R. Iguchi, and K.-i. Uchida, *Phys. Rev. Applied* **11**, 034022 (2019).
- [25] J. Wang, Y. K. Takahashi, and K.-i. Uchida, *Nat. Commun.* **11**, 2 (2020).
- [26] F. Zhang and C.-a. Di, *Chem. Mater.* **32**, 2688 (2020).
- [27] X. Hu, X. Gong, M. Zhang, H. Lu, Z. Xue, Y. Mei, P. K. Chu, Z. An, and Z. Di, *Small* **16**, 1907170 (2020).
- [28] W. A. Hubbard, M. Mecklenburg, J. J. Lodico, Y. Chen, X. Y. Ling, R. Patil, W. A. Kessel, G. J. K. Flatt, H. L. Chan, B. Vareskic, G. Bal, B. Zutter, and B. C. Regan, *ACS Nano* **14**, 11510 (2020).
- [29] R. Landauer, *IBM J. Res. Dev.* **1**, 223 (1957).
- [30] M. Büttiker, Y. Imry, R. Landauer, and S. Pinhas, *Phys. Rev. B* **31**, 6207 (1985).
- [31] W. R. Frensley, *Rev. Mod. Phys.* **62**, 745 (1990).
- [32] Y. Meir and N. S. Wingreen, *Phys. Rev. Lett.* **68**, 2512 (1992).
- [33] Y. Meir, N. S. Wingreen, and P. A. Lee, *Phys. Rev. Lett.* **70**, 2601 (1993).
- [34] A.-P. Jauho, N. S. Wingreen, and Y. Meir, *Phys. Rev. B* **50**, 5528 (1994).
- [35] C. W. J. Beenakker, *Rev. Mod. Phys.* **69**, 731 (1997).
- [36] Y. Imry, *Introduction to Mesoscopic Physics*, Oxford University Press, Oxford, 1997.
- [37] G. Dresselhaus, M. S. Dresselhaus, and R. Saito, *Physical Properties of Carbon Nanotubes*, Imperial College Press, London, 1998.
- [38] A. Nitzan and M. A. Ratner, *Science* **300**, 1384 (2003).
- [39] M. Galperin, A. Nitzan, and M. A. Ratner, *Phys. Rev. Lett.* **96**, 166803 (2006).
- [40] M. Galperin, M. A. Ratner, and A. Nitzan, *J. Phys.: Condens. Matt.* **19**, 103201 (2007).
- [41] M. Di Ventra, *Electrical Transport in Nanoscale Systems*, Cambridge University Press, Cambridge, 2008.
- [42] Z. Ioffe, T. Shamaï, A. Ophir, G. Noy, I. Yutsis, K. Kfir, O. Cheshnovsky, and Y. Selzer, *Nat. Nanotechnol.* **3**, 727 (2008).
- [43] D. R. Ward, D. A. Corley, J. M. Tour, and D. Natelson, *Nat. Nanotechnol.* **6**, 33 (2011).
- [44] X. Zeng, L. Ye, D. Zhang, R.-X. Xu, X. Zheng, and M. Di Ventra, *Phys. Rev. B* **103**, 085411 (2021).
- [45] Y. M. Zuev, W. Chang, and P. Kim, *Phys. Rev. Lett.* **102**, 096807 (2009).
- [46] P. Wei, W. Bao, Y. Pu, C. N. Lau, and J. Shi, *Phys. Rev. Lett.* **102**, 166808 (2009).
- [47] J. G. Checkelsky and N. P. Ong, *Phys. Rev. B* **80**, 081413(R) (2009).
- [48] D. Zhang, X. Zheng, and M. Di Ventra, *Phys. Rep.* **830**, 1 (2019).
- [49] See Supplemental Material at <http://link.aps.org/supplemental> for details about the determination of local temperature and local chemical potential, and the energy spectra of electric and heat currents.
- [50] J. M. Ziman, *Electrons and Phonons: The Theory of Transport Phenomena in Solids*, Oxford University Press, Oxford, 2001.

- [51] M. Wierzbicki and R. Świrakowicz, *Phys. Rev. B* **82**, 165334 (2010).
- [52] B. Dong and X. L. Lei, *J. Phys.: Condens. Matter* **14**, 11747 (2002).
- [53] L. Z. Ye, D. Hou, R. Wang, D. Cao, X. Zheng, and Y. J. Yan, *Phys. Rev. B* **90**, 165116 (2014).
- [54] D. Goldhaber-Gordon, H. Shtrikman, D. Mahalu, D. Abusch-Magder, U. Meirav, and M. A. Kastner, *Nature* **391**, 156 (1998).
- [55] S. M. Cronenwett, T. H. Oosterkamp, and L. P. Kouwenhoven, *Science* **281**, 540 (1998).
- [56] M. Eto and Y. V. Nazarov, *Phys. Rev. Lett.* **85**, 1306 (2000).
- [57] M. Pustilnik and L. I. Glazman, *Phys. Rev. Lett.* **87**, 216601 (2001).
- [58] A. Fuhrer, T. Ihn, K. Ensslin, W. Wegscheider, and M. Bichler, *Phys. Rev. Lett.* **93**, 176803 (2004).
- [59] H. B. Heersche, Z. de Groot, J. A. Folk, L. P. Kouwenhoven, H. S. J. van der Zant, A. A. Houck, J. Labaziewicz, and I. L. Chuang, *Phys. Rev. Lett.* **96**, 017205 (2006).
- [60] P. P. Baruselli, A. Smogunov, M. Fabrizio, and E. Tosatti, *Phys. Rev. Lett.* **108**, 206807 (2012).
- [61] A. Svilans, M. Josefsson, A. M. Burke, S. Fahlvik, C. Thelander, H. Linke, and M. Leijnse, *Phys. Rev. Lett.* **121**, 206801 (2018).
- [62] P. Jarillo-Herrero, J. Kong, H. S. J. van der Zant, C. Dekker, L. P. Kouwenhoven, and S. De Franceschi, *Nature* **434**, 484 (2005).
- [63] M.-S. Choi, R. López, and R. Aguado, *Phys. Rev. Lett.* **95**, 067204 (2005).
- [64] R. M. Potok, I. G. Rau, H. Shtrikman, Y. Oreg, and D. Goldhaber-Gordon, *Nature* **446**, 167 (2007).
- [65] F. Kuemmeth, S. Ilani, D. C. Ralph, and P. L. McEuen, *Nature* **452**, 448 (2008).
- [66] T.-F. Fang, W. Zuo, and H.-G. Luo, *Phys. Rev. Lett.* **101**, 246805 (2008).
- [67] M. Karolak, D. Jacob, and A. I. Lichtenstein, *Phys. Rev. Lett.* **107**, 146604 (2011).
- [68] S. Amasha, A. J. Keller, I. G. Rau, A. Carmi, J. A. Katine, H. Shtrikman, Y. Oreg, and D. Goldhaber-Gordon, *Phys. Rev. Lett.* **110**, 046604 (2013).
- [69] P. W. Anderson, *Phys. Rev.* **124**, 41 (1961).
- [70] Y. Tanimura and R. Kubo, *J. Phys. Soc. Jpn.* **58**, 101 (1989).
- [71] J. Jin, X. Zheng, and Y. J. Yan, *J. Chem. Phys.* **128**, 234703 (2008).
- [72] Z. H. Li, N. H. Tong, X. Zheng, D. Hou, J. H. Wei, J. Hu, and Y. J. Yan, *Phys. Rev. Lett.* **109**, 266403 (2012).
- [73] L. Ye, X. Wang, D. Hou, R.-X. Xu, X. Zheng, and Y. J. Yan, *WIREs Comput. Mol. Sci.* **6**, 608 (2016).
- [74] L. Han, H.-D. Zhang, X. Zheng, and Y. J. Yan, *J. Chem. Phys.* **148**, 234108 (2018).
- [75] L. Cui, H.-D. Zhang, X. Zheng, R.-X. Xu, and Y. J. Yan, *J. Chem. Phys.* **151**, 024110 (2019).
- [76] H.-D. Zhang, L. Cui, H. Gong, R.-X. Xu, X. Zheng, and Y. J. Yan, *J. Chem. Phys.* **152**, 064107 (2020).
- [77] X. Zheng, Y. J. Yan, and M. Di Ventura, *Phys. Rev. Lett.* **111**, 086601 (2013).
- [78] X. Wang, L. Yang, L. Ye, X. Zheng, and Y. J. Yan, *J. Phys. Chem. Lett.* **9**, 2418 (2018).
- [79] X. Li, L. Zhu, B. Li, J. Li, P. Gao, L. Yang, A. Zhao, Y. Luo, J. Hou, X. Zheng, B. Wang, and J. Yang, *Nat. Commun.* **11**, 2566 (2020).
- [80] X. Li, H. Gong, Q. Zhuang, B. Wang, X. Zheng, and J. Yang, *J. Phys. Chem. C* **125**, 21488 (2021).
- [81] Y. Tanimura, *J. Chem. Phys.* **153**, 020901 (2020).
- [82] L. Z. Ye, D. Hou, X. Zheng, Y. J. Yan, and M. Di Ventura, *Phys. Rev. B* **91**, 205106 (2015).
- [83] L. Z. Ye, X. Zheng, Y. J. Yan, and M. Di Ventura, *Phys. Rev. B* **94**, 245105 (2016).
- [84] J. P. Bergfield, S. M. Story, R. C. Stafford, and C. A. Stafford, *ACS Nano* **7**, 4429 (2013).
- [85] J. P. Bergfield, M. A. Ratner, C. A. Stafford, and M. Di Ventura, *Phys. Rev. B* **91**, 125407 (2015).
- [86] A. Shastry and C. A. Stafford, *Phys. Rev. B* **94**, 155433 (2016).
- [87] A. Shastry, S. Inui, and C. A. Stafford, *Phys. Rev. Applied* **13**, 024065 (2020).
- [88] S. De Franceschi, R. Hanson, W. G. van der Wiel, J. M. Elzerman, J. J. Wijkema, T. Fujisawa, S. Tarucha, and L. P. Kouwenhoven, *Phys. Rev. Lett.* **89**, 156801 (2002).
- [89] A. Altland and R. Egger, *Phys. Rev. Lett.* **102**, 026805 (2009).
- [90] G. Cohen, E. Gull, D. R. Reichman, and A. J. Millis, *Phys. Rev. Lett.* **112**, 146802 (2014).
- [91] A. E. Antipov, Q. Dong, and E. Gull, *Phys. Rev. Lett.* **116**, 036801 (2016).